GEM TN-92-92

Simulations of Accordion EM Calorimeters

Hong Ma
Brookhaven National Laboratory

April 27, 1992

Abstract:

This is a summary of the GEANT simulation of the non-projective accordion EM calorimeters. Most of the simulations are related to the prototype stacks that are being built at BNL. EM shower resolution, position resolution, γ — π^o separation, chevron electrodes, resolution at large incident angle and effect of the cryostat walls are discussed.

Simulations of Accordion EM calorimeters

Hong Ma

Brookhaven National Laboratory

April 27, 1992

This is a summary of the GEANT simulation of the non-projective accordion EM calorimeters. Most of the simulations are related to the prototype stacks that are being built at BNL. EM shower resolution, position resolution, $\gamma - \pi^0$ separation, chevron electrodes, resolution at large incident angle and effect of the cryostat walls are discussed.

1 Accordion calorimeter and simulation

The accordion EM calorimeter was first proposed at CERN and tested in 1990 and 1991. The main advantages are better signal connection for fast readout and hermeticity. A detailed description of the previous simulations is given in Ref 1, and experimental data are presented in Ref 2.

Fig 1 and 2 show the cross section of an accordion calorimeter. A cell in x is defined as the region from the middle of the absorber plate to the middle of the next absorber plate with 0 at the center. With the given geometry (half a bend at the beginning and the end of the stack), the center of the cell is also the same as the mean position of the cell. A supercell is an actual readout channel which consists of three cells. A slice is a division in y with given width. In the simulation, the stack is normally longitudinally divided into three equal sections, with the front one being one readout, and the other two being the other readout.

In the shower simulation, the incident particles are normally randomly sprayed across one readout channel (one slice, and three cells).

The simulations are done in the SGI machines at SSCL and BNL. The GEANT energy cut parameters are set to 10 keV. The CPU time per event is about 120 seconds

at 10 GeV. Most of runs of the simulation contain 1000 events. Therefore, a statistical error of about 3% should be attached to most of the numbers.

The accordion GEANT code was originally developed by M. Lefebvre. Some modifications are made to simulate the 1mm option, chevron electrodes, and etc.

In most of the simulations, electronic noise has not be taken into account. A cryostat of $0.8X_0$ thick is included in all the simulations.

The dimensions of the stack in construction are 21 cells in x and 37.5cm in y with 16 accordion bends.

2 Design of the test stacks

It has been proposed to improve the EM resolution of the accordion calorimeter designed and tested at CERN by two possible methods. One is to replace Ar with Kr while reducing the absorber thickness (2mm option). The other is to double the sampling frequency while keeping the same sampling ratio (1mm option). This is achieved by using Pb as electrodes, while reducing the Pb thickness by a factor of two.

Parameter	CERN RD3	2mm	1mm	comments
Pb absorber (mm)	1.8	1.3	0.8	
prePrag (mm)	0.1	0.1	0.1	×2
Fe cladding (mm)	0.1	0.2	0.2	×2
electrode (mm)	0.07 (Cu)	0.07 (Cu)	0.8 (Pb)	
Kapton (mm)	.165	.165	.2	×2
argon (mm)	1.9	2.05	1.9	×2
total (mm)	6.4	6.40	6.4	
pitch (mm)	4.01	4.01	4.01	
mean radius (mm)	3.	3.	3.	absorber and electrode
total X_0	25.3(Ar)	24.2(Kr)	23.4(Ar)	

Table 1: Accordion calorimeter parameters

Using the accordion GEANT code, the parameters for the stacks are determined.

Table 1 lists all the parameters for the CERN RD3 design and our 1mm and 2mm options. The pitch (the bend to bend distance) and mean radius of each bend are the same as the CERN design because the same bending machine is used. For the 2mm option, the Pb absorber thickness is reduced from 1.8mm to 1.3mm while the stainless steel thickness is increased to 2mm for mechanical considerations. The electrode thickness remains the same. The liquid thickness is determined by the requirement that response to electron showers be as uniform as possible within a cell. This can be first optimized by ray tracing using the geantino in GEANT (a particle that does not interact with matter, but is used to trace through the calorimeter to check the geometry, to calculate the path length or radiation length, etc) to calculate the fluctuation of the sampling ratio. Figure 3 shows the liquid radiation length divided by the total radiation length as a function of position in a cell (this ratio is proportional to the sampling ratio), for four different liquid thicknesses. The fluctuation in the middle of the cell comes from the imperfect matching of the corners of the accordion bends with finite curvature. Figure 4 shows the uniformity of the response to 10 GeV electrons within a cell for the four cases as described above. The non-uniformity is defined as the rms of the sampling ratio in each bin (or the average shower response in each bin) of the histogram. The solid points on Figure 5 shows the non-uniformity (rms) as a function of the liquid gap thickness. It also shows how sensitive the uniformity of response to the liquid thickness. The configuration with the least variation in sampling ratio does not necessarily correspond to the best configuration for the showers because of the finite size of the showers.

The thickness of the absorber at the corner, as measurement on a sample made a BNL, is about 5 mils thinner than the thickness at the straight section. This deviation from ideal configuration will affect the uniformity, for better or for worse. This effect is simulation with a thinned corner Pb absorber (by 120μm). The open points on Fig 5 shows the non-uniformity of the shower response as a function of liquid gap.

The Kr thickness is chosen to be 2.05mm, inbetween the optimum for ideal and the case with thinned corners. This gives the total cell size of 6.4mm. The final thickness of the liquid gap will depend on the thickness of the real absorber plates and electrodes, with the total cell size fixed.

Similar procedure is applied to 1mm option. The structure of the fluctuation of the sampling ratio within a cell is different from the previous one because of the additional absorber in the electrodes, which adds more fluctuations at the two ends of the cell. Figure 6 shows the sampling ratio as well as the shower response for two configurations.

The Pb in the electrode has to be strips, with some separation between the strips. This results in an increase of sampling ratio near the edges of the strips. Figure 7 shows the response to electron showers as a function of y in a slice. Although the increase in response at the edges (y=$\pm$0.5$\times$cell_size) is noticeable, it doesn't deteriorate the resolution by much ($\leq$ .3%), and can be corrected if it is necessary.

The resolutions of electron showers of 10 GeV are summarized in Table 2.

Cells	CERN RD3	2mm	1mm
3 $\times$ 3	2.82	2.35	2.11
5 $\times$ 5	2.65	2.07	1.96
Total	2.52	1.85	1.89

Table 2: Electron energy resolution(σ/E in %) at 10 GeV, GEANT simulation.

3 Position resolution and chevron electrodes

The accordion has excellent position resolution in x (the bending direction) because of the shower sharing between the neighboring cells. It is designed such that a particle at 0 incident angle traversing the calorimeter without multiple scattering will only deposit energy in two neighboring readout cells. The position can be calculated by simply the first moment with energy weighting. Figure 8a shows the calculated position vs the impact point. Figure 8b shows the position resolution.

The other projection, y, is similar to normal modular EM calorimeters. That is, the position calculated by first moment with energy weighting (y_r) is not linear with the impact position. Figure 8c shows the calculated position vs the impact point. A correction has to be applied. A simple formula $y_c = \alpha \cdot arctan(\beta y_r)$ is sufficient to describe the dependence, where α and β can be determined from the Monte Carlo events. Figure 8d shows the resolution after the correction. The y resolution after correction actually varies significantly as a function of the impact point (Fig 9), while the x resolution is independent of the impact point. The average y resolution after correction is not as good as the x resolution.

By modifying the electrodes to allow energy sharing between neighboring slices, the position resolution in y can be improved. The simplest configuration is to shift the

electrode back and forth by one slice in the same frequency as the accordion bends. This means that the bends in x and y directions are fully correlated. For particles without multiple scattering, the fluctuation in the position measurement in x and y are fully correlated because the fluctuation comes only from the fluctuation of the dE/dx energy loss. In the measurement of the shower position, however, the fluctuation comes mainly from the multiple scattering of the particles. As the shower simulation shows, there is no correlation at all between the x and y measurements. With this configuration, the position resolution of y is identical to that of x.

Table 3 shows the position resolution of 10 GeV electrons in x, and y with regular and chevron electrodes. The rms_y is the rms of the y measurements before the correction, since the distribution is non-gaussian. The improvement in position resolution by the chevron electrodes is more significant when the slice width becomes larger. This may help us save the number of channels without losing the position resolution.

Cell size(mm)	σ_x(mm)	rms_y (mm)	σ_y^{corr}(mm)	$\sigma_y^{chevron}$(mm)
27	1.02	3.38	1.15	1.07
35		4.73	1.45	1.04

Table 3: Position resolution of accordion calorimeter, 10 GeV electrons, GEANT simulations.

Another concern about the chevron electrode is the additional energy spread among the neighboring cells. With the cell size of 27mm, the distribution of the energy in 3×3 cells divided by the energy in 5×5 cells is almost the same for slice and chevron electrodes (Figure 10). Therefore, the chevron electrode does not increase the measured shower size. Isolation cuts can still be used.

With the longitudinal division of the calorimeter, the matching of the positions in depth may be used to reject background or to measure the direction of the shower. However, care has to be taken when accordion (or chevron) is used for truncated showers. Because the size of the accordion bends is not small compared to the shower size, the position measurement of a truncated shower is biased. In addition, the longitudinal shower fluctuation will worsen the position resolution of a truncated shower. Figure 11 shows x_1-x_{impact} (x_1 is the measurement from the front 1/3 of the calorimeter), x_2-x_{impact} (x_2 is the measurement from the back 2/3 of the calorimeter) and x_1-x_2. The bias depends on where the calorimeter is divided, and on the average longitudinal

shower shape, which is related to the particle energy as well as particle type. x1 and x2 are anticorrelated.

With the known particle species, x_1-x_2 can still be used to determined the direction of the shower. Fig 12 shows x_1-x_2 as a function of the incident angle for electrons at 10 GeV. Also shown is x1-x2 at zero incident angle for some other energies and other particles, as well as some other longitudinal division of the stack. The variation of the bias is about 4.7mm for different longitudinal divisions of the calorimeter, and about .32mm for electrons and photons of 10-40 GeV. More variation is possible for higher energy or other particles.

4 $\gamma - \pi^0$ separation

The shower shape of π^0's, when the separation of the two photons are sufficient, is different from that of single photons. The rms of the shower, defined as,

$$rms_x = \sqrt{\frac{\sum E_i x_i^2}{\sum E_i} - (\frac{\sum E_i x_i}{\sum E_i})^2},$$

in both x and y projections can be used to characterize the shower size. However, the rms is not uniform within a cell, in either x or y. This modulation within a cell can be parameterized as $rms_x = A_x + B_x cos(C_x x_r)$ (similar formula for y) where the parameters can be determined from the Monte Carlo events. Figure 13 shows the variation of rms_x (rms_y) in a cell and the fit. To minimize the fluctuation of rms, the modulation is then taken out by subtracting the second term from the measured rms. The shower size is then defined as $r = \sqrt{(rms_x^{corr}/\overline{rms_x})^2 + (rms_y^{corr}/\overline{rms_y})^2}$ where $\overline{rms}$ is the mean rms for each projection. The same parameters determined with the photon showers of a given energy are used for the π^0 showers of the same energy. The distribution of the variable r is then used to discriminate π^0's from photons. Figure 14a shows the r distribution for 10 GeV photons and π^0's (vertex at 75 cm in front of the calorimeter), while Figure 14b is the integral from the left of the histogram above. With the photon efficiency fixed at 90%, Figure 15 shows the π^0 acceptance as a function of the energy. It is should be noted that with this method, chevron electrode can do just as well as the regular electrodes. From this, we may probably say that the accordion structure does not prevent us from using the shower shape analysis.

The photons from π^0 decays have minimum opening angle when they have the same energy. As the separation becomes larger, the energies of the two photons becomes very asymmetric. The rejection of π^0's depends not only on the separation of the photons,

but also the energy ratio of the photons.

Although the calorimeter, at the distance of 75cm from the colliding beams as constrained by the GEM detector, is not useful in rejecting high energy (> 20 GeV) π^0's, the shower shape analysis may still be helpful in rejecting other backgrounds such as multiple π^0 from jet fragmentation.

5 Resolution at large incident angle

At the end of the barrel calorimeter, the incident angle is large ($\geq 45°$). While the sampling ratio remains the same as the incident angle increases, the resolution tends to get worse. There are three major effects. First, along the incident particle direction, the sampling frequency is lower when the incident angle is large. To isolate this effect, we use a parallel plate geometry with absorber and signal electrode material identical to the accordion. Fig 16 shows the resolution ($\sigma_E/\sqrt{E}$) as a function of η (the three different points corresponds to incident angle =0, 45 and 60 degrees). Two different thicknesses are considered, one is the same as the 2mm option, the other has all the thickness increased by a factor of $\sqrt{2}$. Because the shower at the shower center is close to isotropic, resolution does not scale with the apparent sampling frequency.

Second, the sampling ratio in an accordion calorimeter is modulated longitudinally by the bends. A large sampling in one corner region is compensated by the absorber in the corner region of the next bend. At normal incidence, each bend is about 1.5 radiation length apart. At an incident angle of 60 degrees, this is doubled. As a result, this signal is more sensitive to longitudinal fluctuation, the non-uniformity is large, and the resolution is worse. In order to preserve the resolution at the large incident angle, it has been suggested that the absorber be thinned in the forward region of the barrel calorimeter. This can be achieved by replacing the 1.3mm Pb with 0.9mm Pb cladded with 0.2mm stainless steel on each side. The total thickness of the absorber plate remains the same. Fig 17 shows the resolution as a function of η for Pb thickness of 1.3mm and 0.9mm Pb, after subtracting the contribution from the non-uniformity. By changing the absorber thickness at about 45 degree of incident angle, one can achieve an acceptable resolution at the forward region.

A similar simulation is done for the 1mm option. It is worth noting that 1mm option is intrinsically more uniform, longitudinally and transversely, than the 2mm option because of the more frequent sampling. Fig 18 shows the resolution as a function of η, without cryostat walls, and with cryostat walls. The non-uniformity is not corrected.

Another effect due to the large incident angle is from the cryostat walls, if the cryostat walls have constant thicknesses. Assuming an inactive material of about $0.5X_0$ in front of the calorimeter, the resolution gets worse by a factor of 1.07 in the forward region. However, one feature of the accordion may be used to reduce this effect. As shown on Fig 2, at the beginning of the accordion calorimeter, there can be a small straight section. It is possible to collect the charge in liquid while replace the absorber with lighter material (such as G10). This is effectively a massless gap with a depth that can be adjusted to compensate the energy loss in the dead material. Fig 19 shows the correlation between the energy loss in the cryostat and the energy measured in the massless gap for 10 GeV electrons. Figure 20 shows the energy distribution with and without the energy measurement in the massless gap, for 10 GeV electrons. This preliminary study shows that with 8mm in depth, part of the resolution, as well as the amplitude, is recovered. Table 4 compares the mean and resolution with different configuration for electron of 10 and 40 GeV at 60 and 45 degrees of incident angles. Within the limit of the statistics (2.2% relative uncertainty on the resolution), the correction works well for the energy and angular range.

		No cryostat		With cryostat		and Massless gap	
E_{el}(GeV)	Angle(°)	E_{Ar} (GeV)	σ/E (%)	E_{Ar} (GeV)	σ/E (%)	E_{Ar} (GeV)	σ/E (%)
40	60	12.63	1.086	12.57	1.181	12.63	1.112
40	45	12.65	0.969	12.61	1.060	12.63	1.015
10	60	3.153	2.160	3.104	2.282	3.143	2.134
10	45	3.158	1.955	3.140	2.022	3.155	1.983

Table 4: Electron signal, with and without cryostat at large incident angle. No correction to the transverse non-uniformity.

It remains to be studied that how this correction varies with the thickness of the cryostat walls, and how effectively the charge in the gap can be collected where the field is lower and non-uniform at the edge.

6 Reference

1) A.Aubert *et al.* (RD3 Collaboration), *Performance of a liquid argon electromag-*

netic calorimeter with an accordion geometry, Nucl. Instr. and Meth,**A309**(1991)138.

2) Michel Lefebvre, Liquid argon accordion Calorimeter simulation, RD3-CAL-No-002

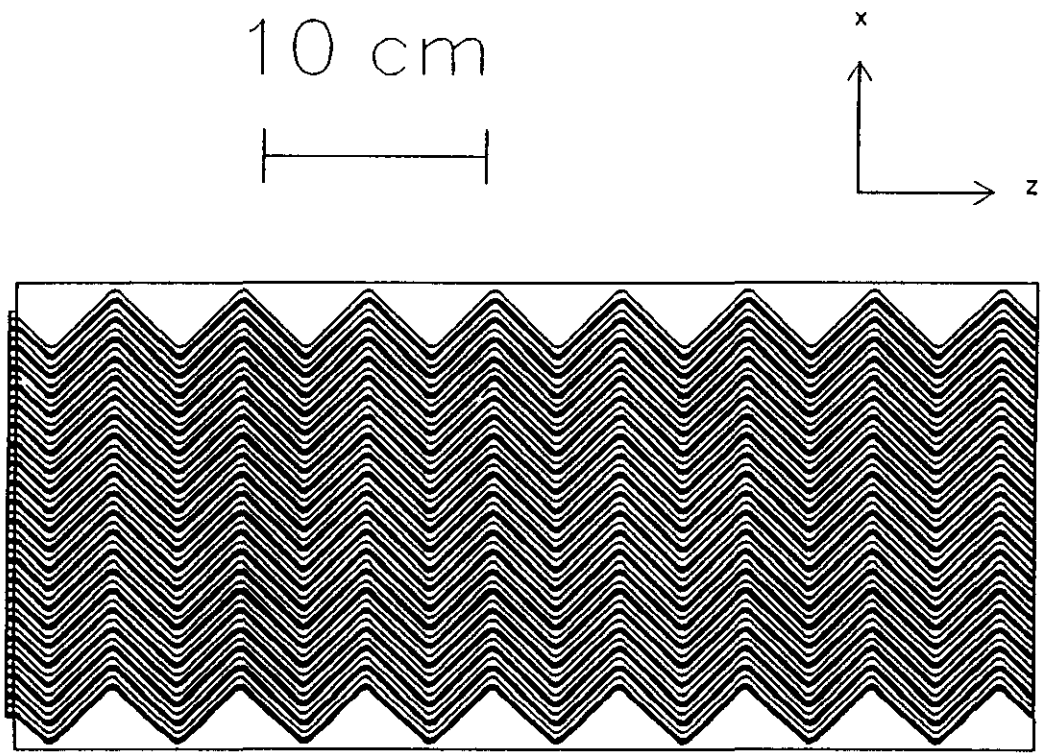

Figure 1

Figure 2

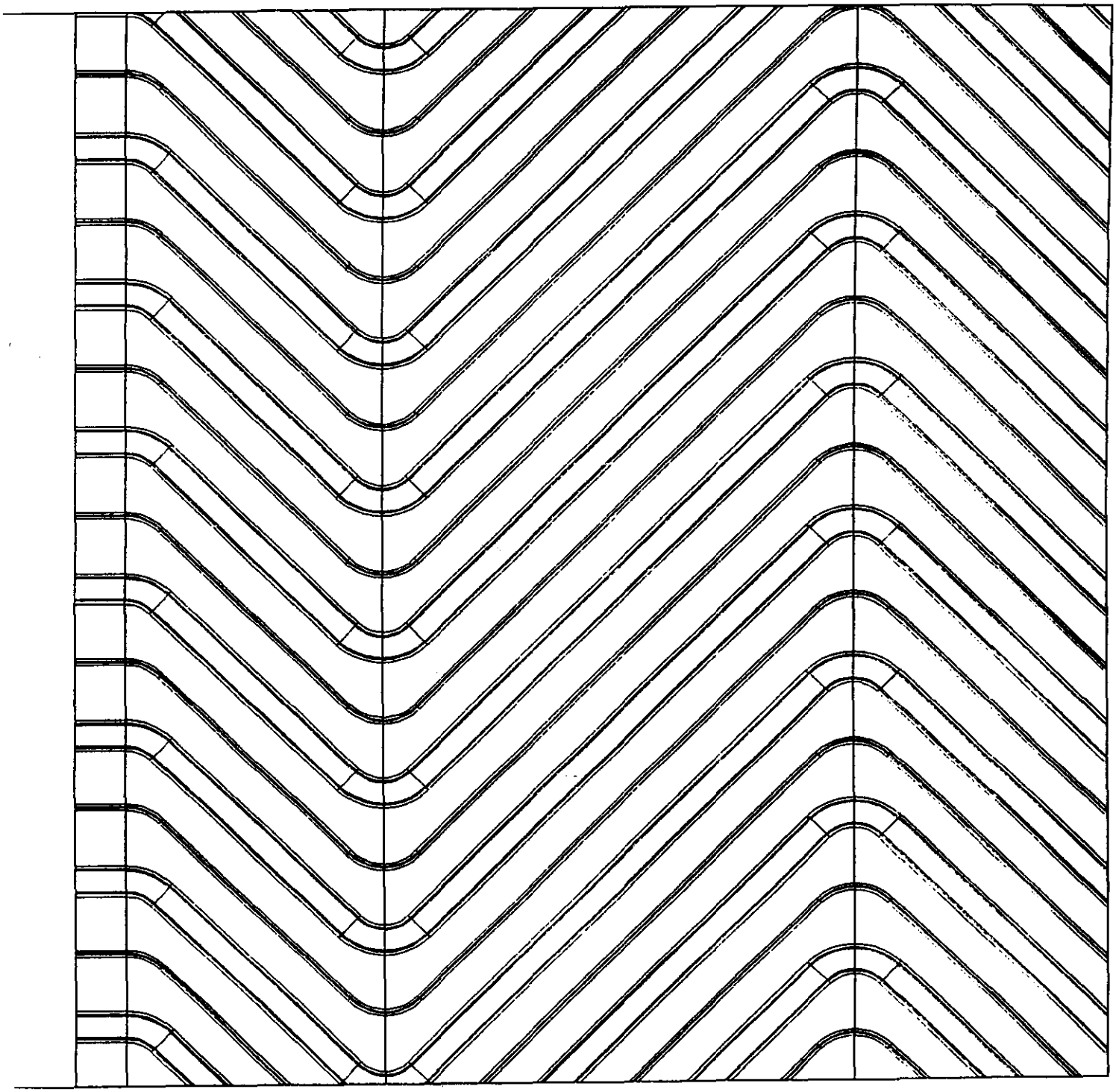

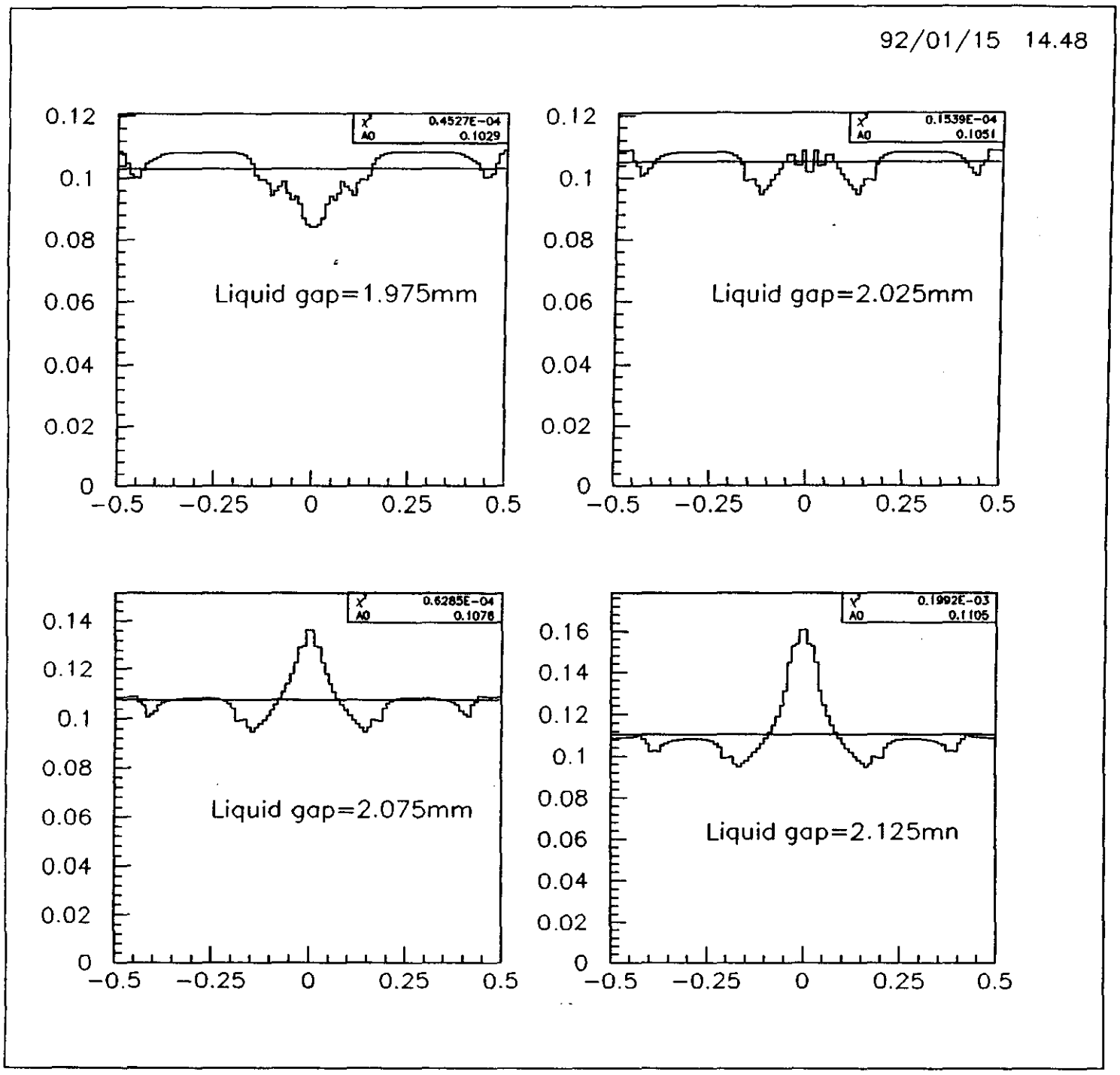
92/01/15 14.48
χ² 0.4527E-04
A0 0.1029
Liquid gap=1.975mm
χ² 0.1539E-04
A0 0.1051
Liquid gap=2.025mm
χ² 0.6285E-04
A0 0.1076
Liquid gap=2.075mm
χ² 0.1992E-03
A0 0.1105
Liquid gap=2.125mn

Figure 3

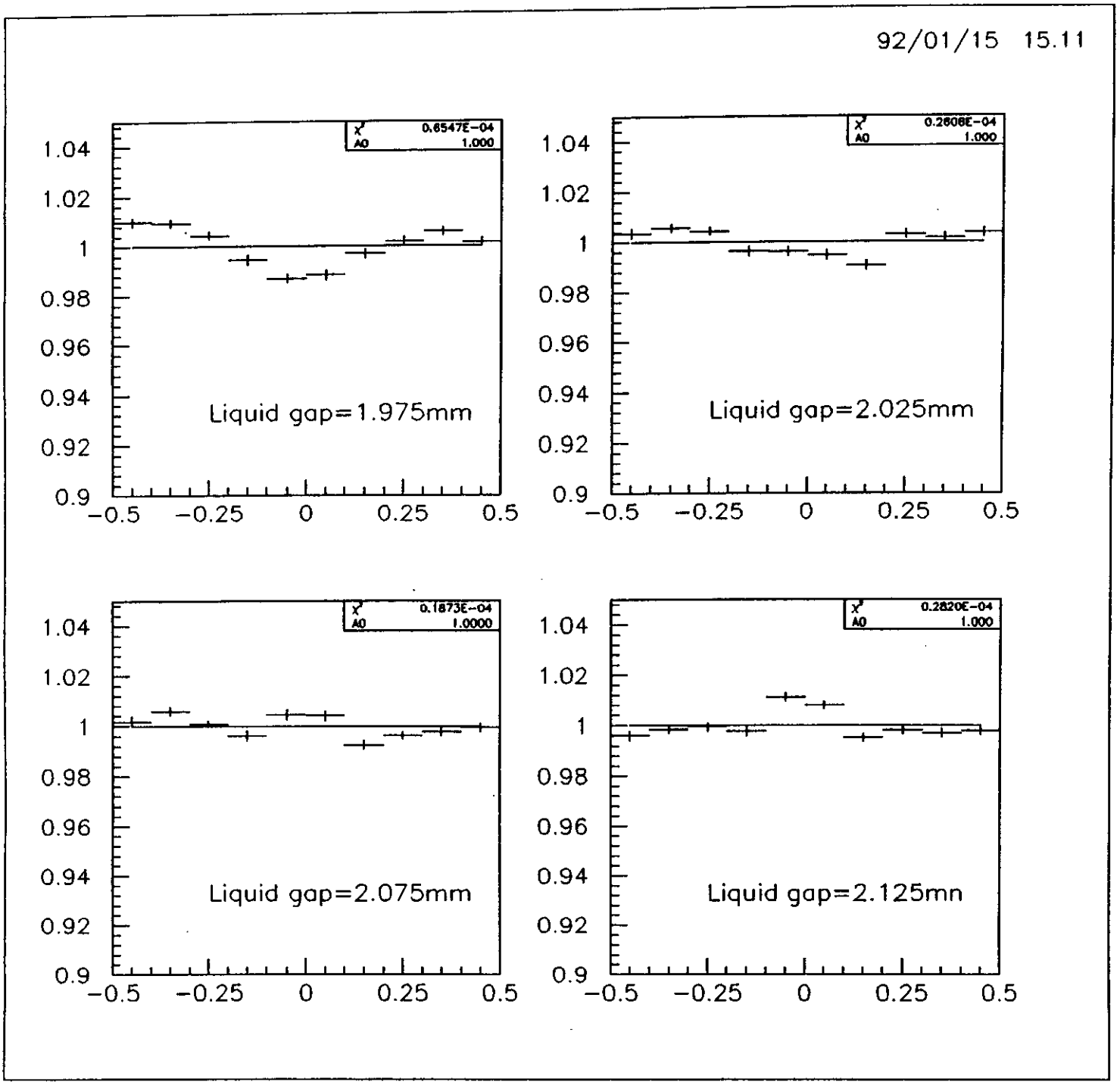
92/01/15 15.11
χ² 0.6547E-04
A0 1.000
Liquid gap=1.975mm
χ² 0.2606E-04
A0 1.000
Liquid gap=2.025mm
χ² 0.1873E-04
A0 1.0000
Liquid gap=2.075mm
χ² 0.2820E-04
A0 1.000
Liquid gap=2.125mn
1.04
1.02
1
0.98
0.96
0.94
0.92
0.9
−0.5
−0.25
0
0.25
0.5

Figure 4

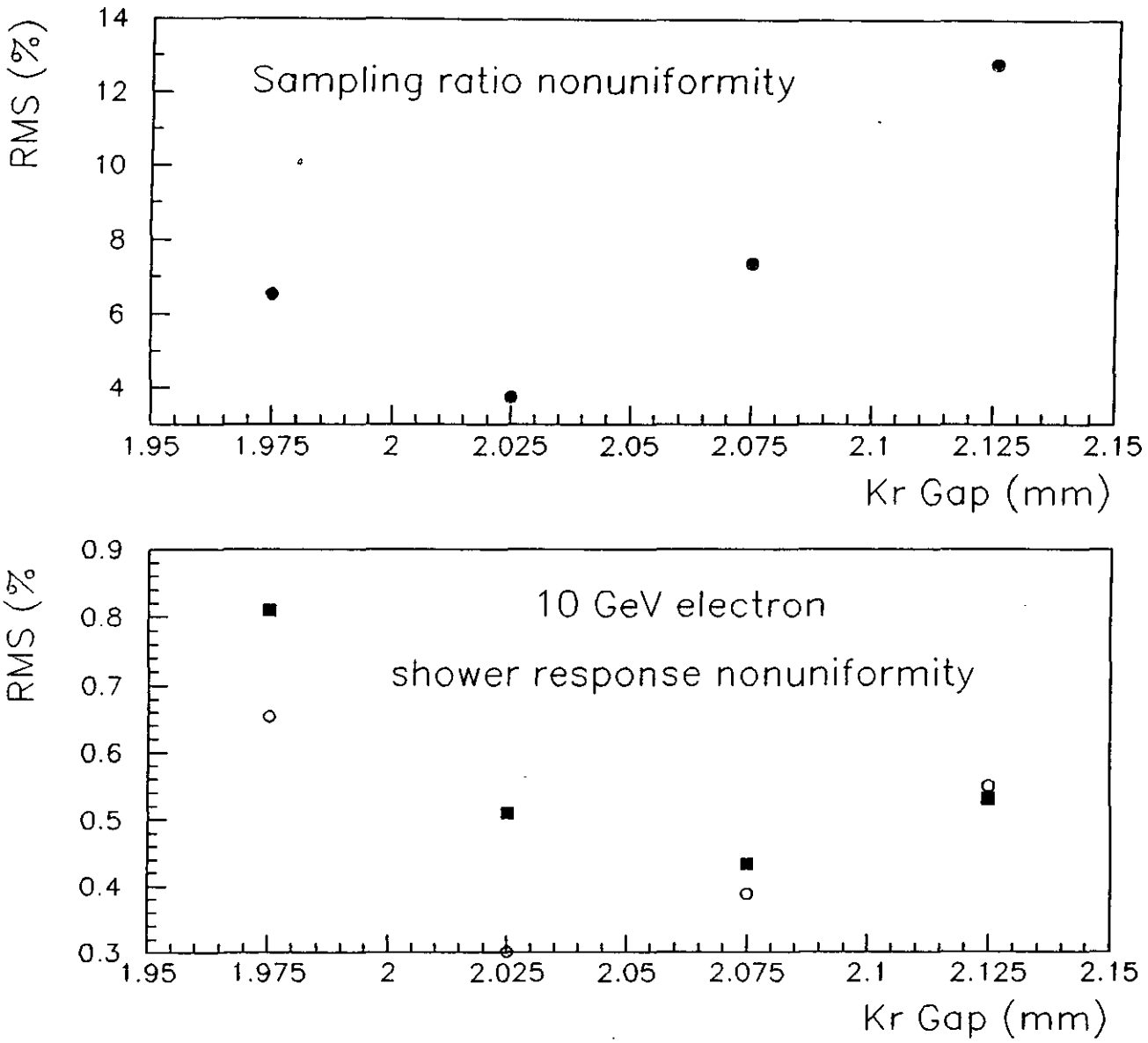
Sampling ratio nonuniformity
RMS (%)
14
12
10
8
6
4
1.95
1.975
2
2.025
2.05
2.075
2.1
2.125
2.15
Kr Gap (mm)
10 GeV electron
shower response nonuniformity
RMS (%
0.9
0.8
0.7
0.6
0.5
0.4
0.3
1.95
1.975
2
2.025
2.05
2.075
2.1
2.125
2.15
Kr Gap (mm)

Figure 5

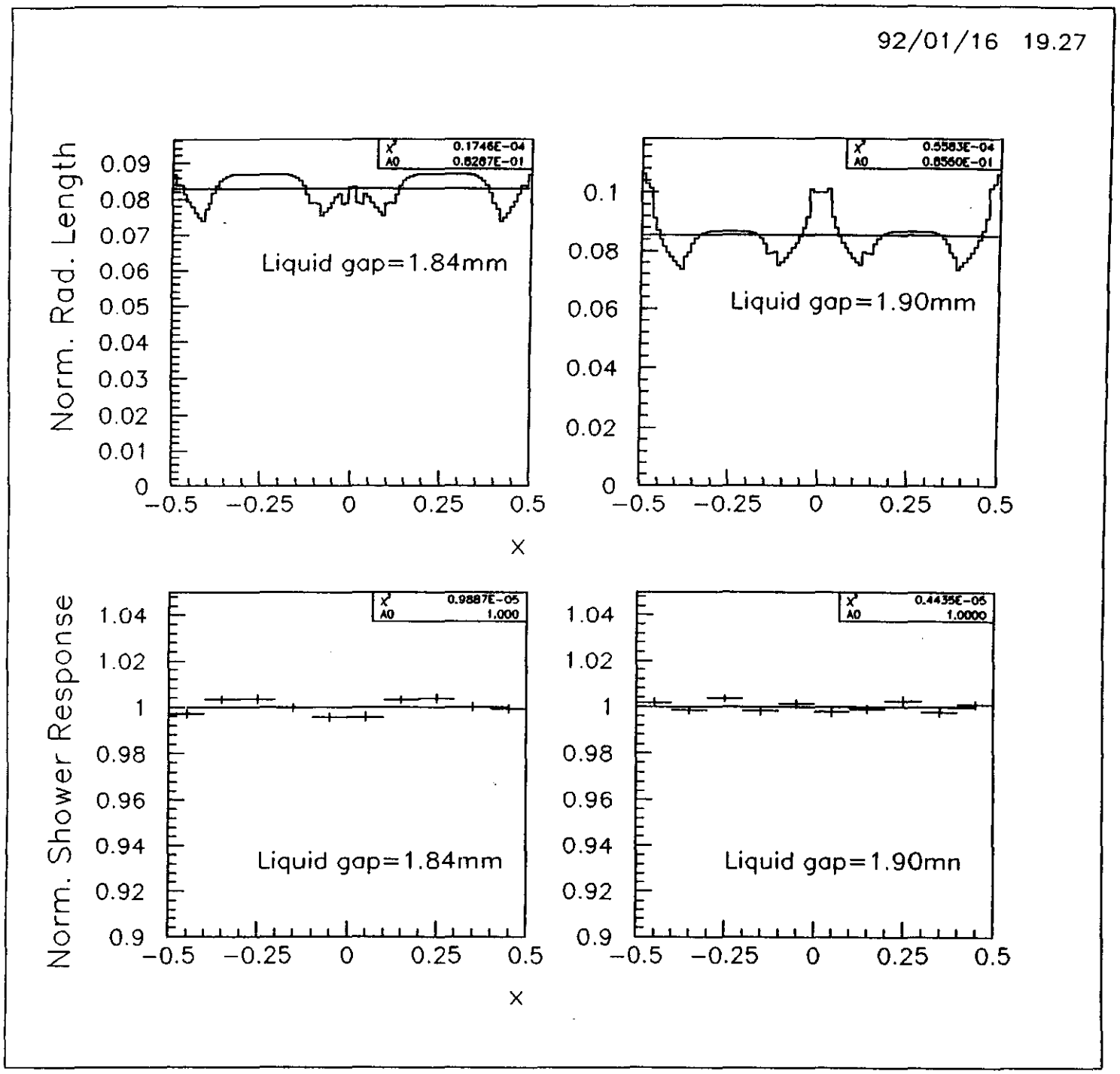
92/01/16 19.27
Norm. Rad. Length
Liquid gap=1.84mm
Liquid gap=1.90mm
Norm. Shower Response
Liquid gap=1.84mm
Liquid gap=1.90mn
X
X

Figure 6

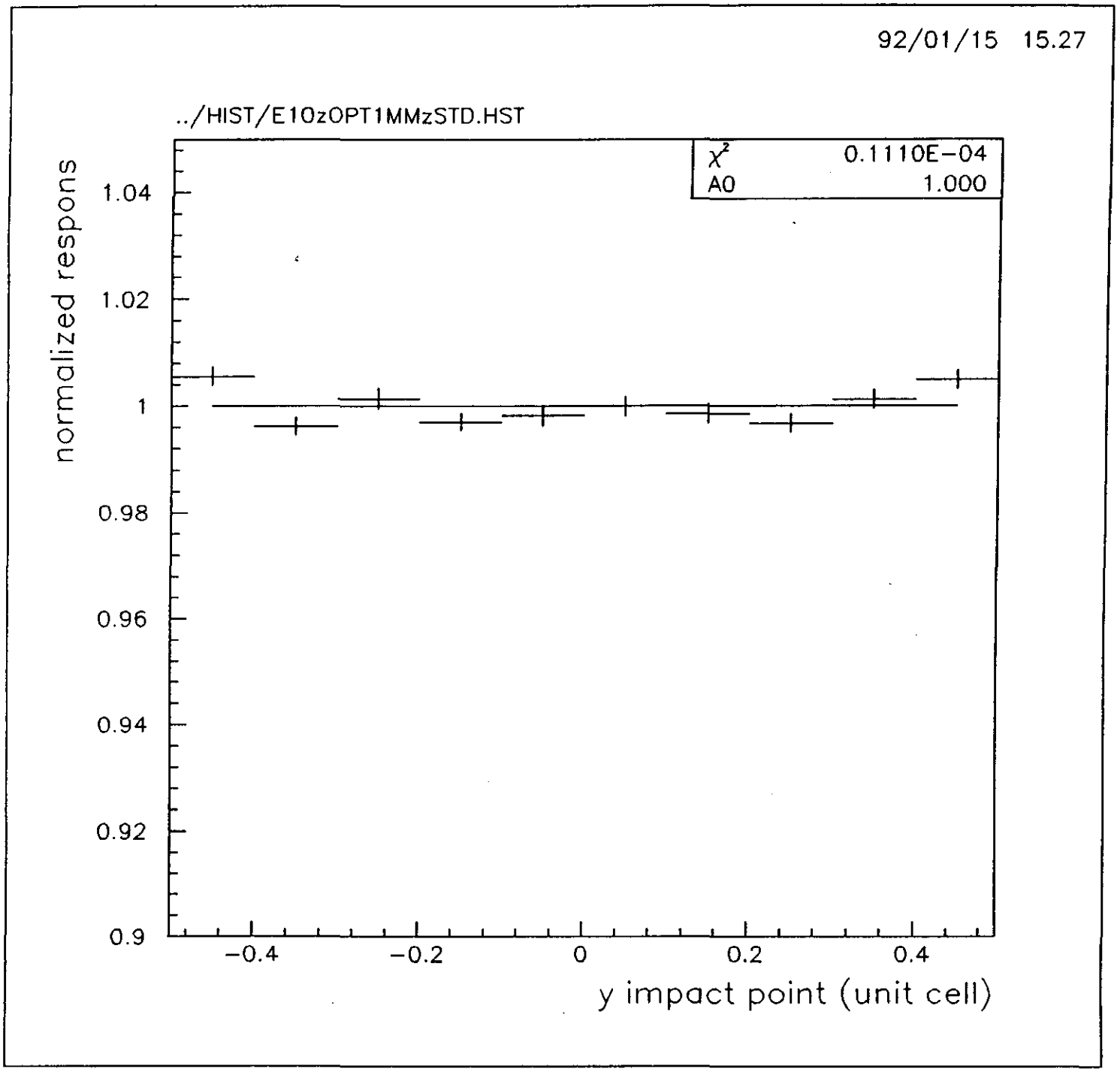
92/01/15 15.27
../HIST/E10zOPT1MMzSTD.HST
χ^2 0.1110E−04
A0 1.000
normalized respons
1.04
1.02
1
0.98
0.96
0.94
0.92
0.9
−0.4
−0.2
0
0.2
0.4
y impact point (unit cell)

Figure 7

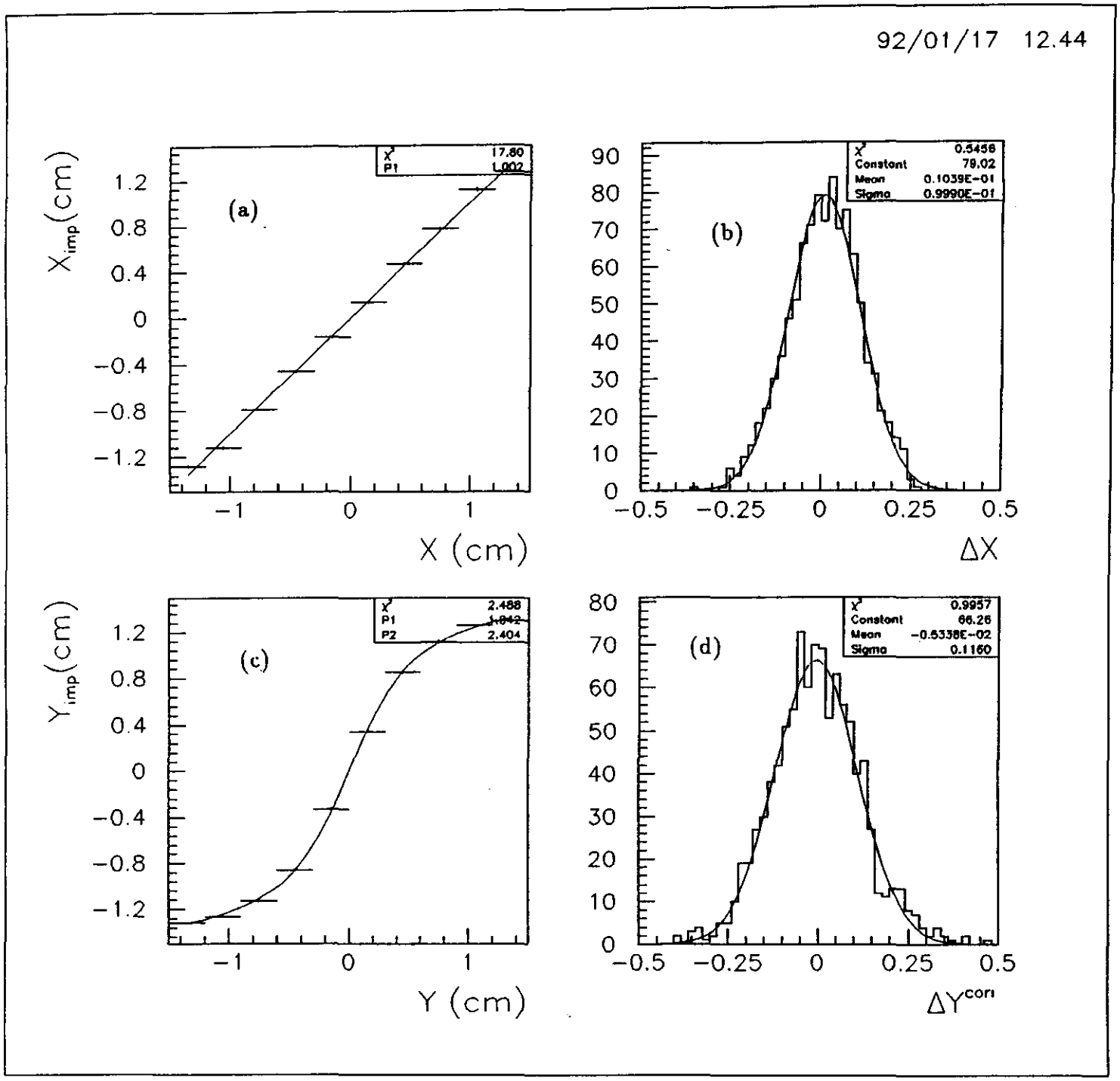

Figure 8

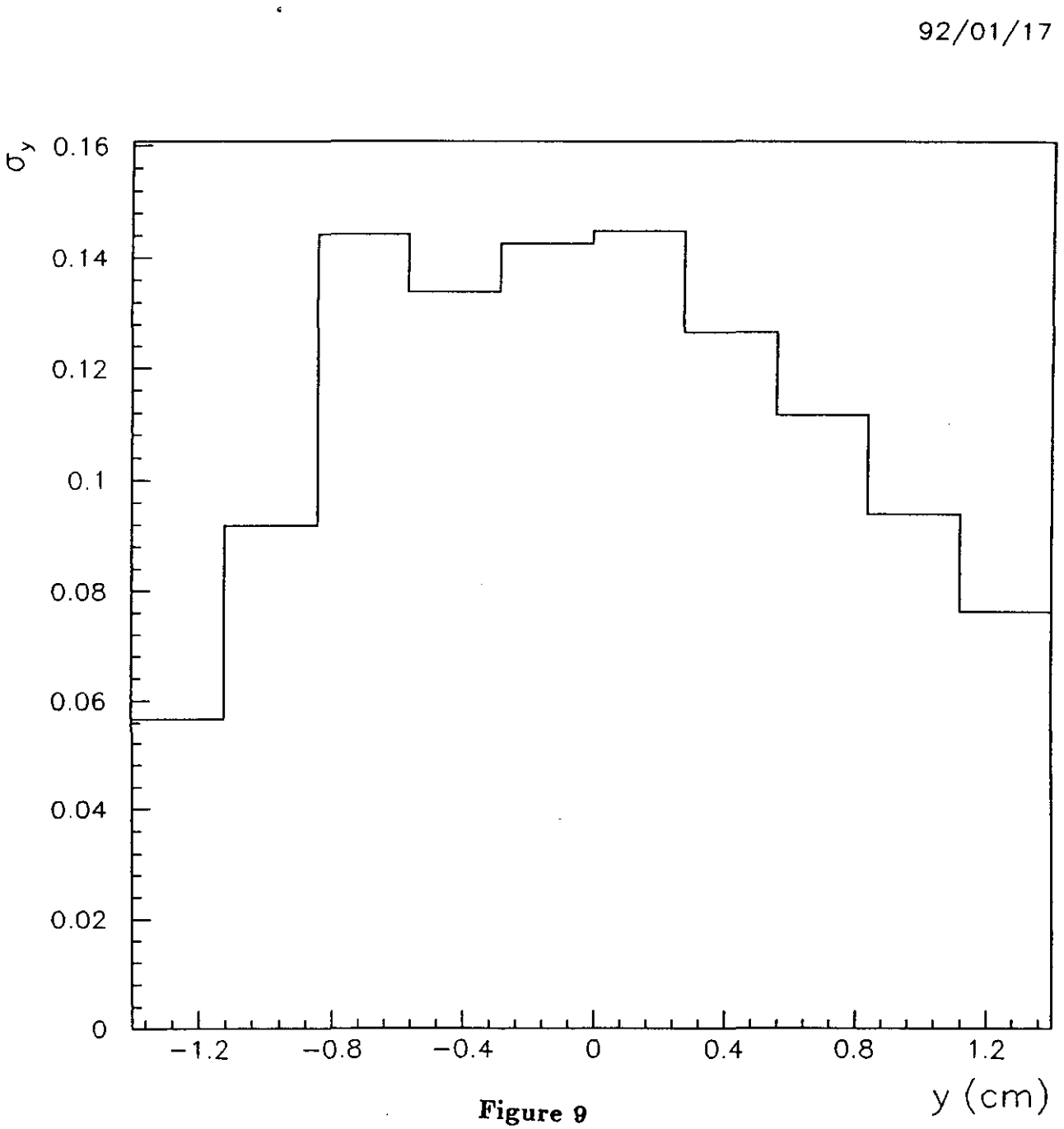
92/01/17 12.24
σ_y
0.16
0.14
0.12
0.1
0.08
0.06
0.04
0.02
0
−1.2
−0.8
−0.4
0
0.4
0.8
1.2
y (cm)

Figure 9

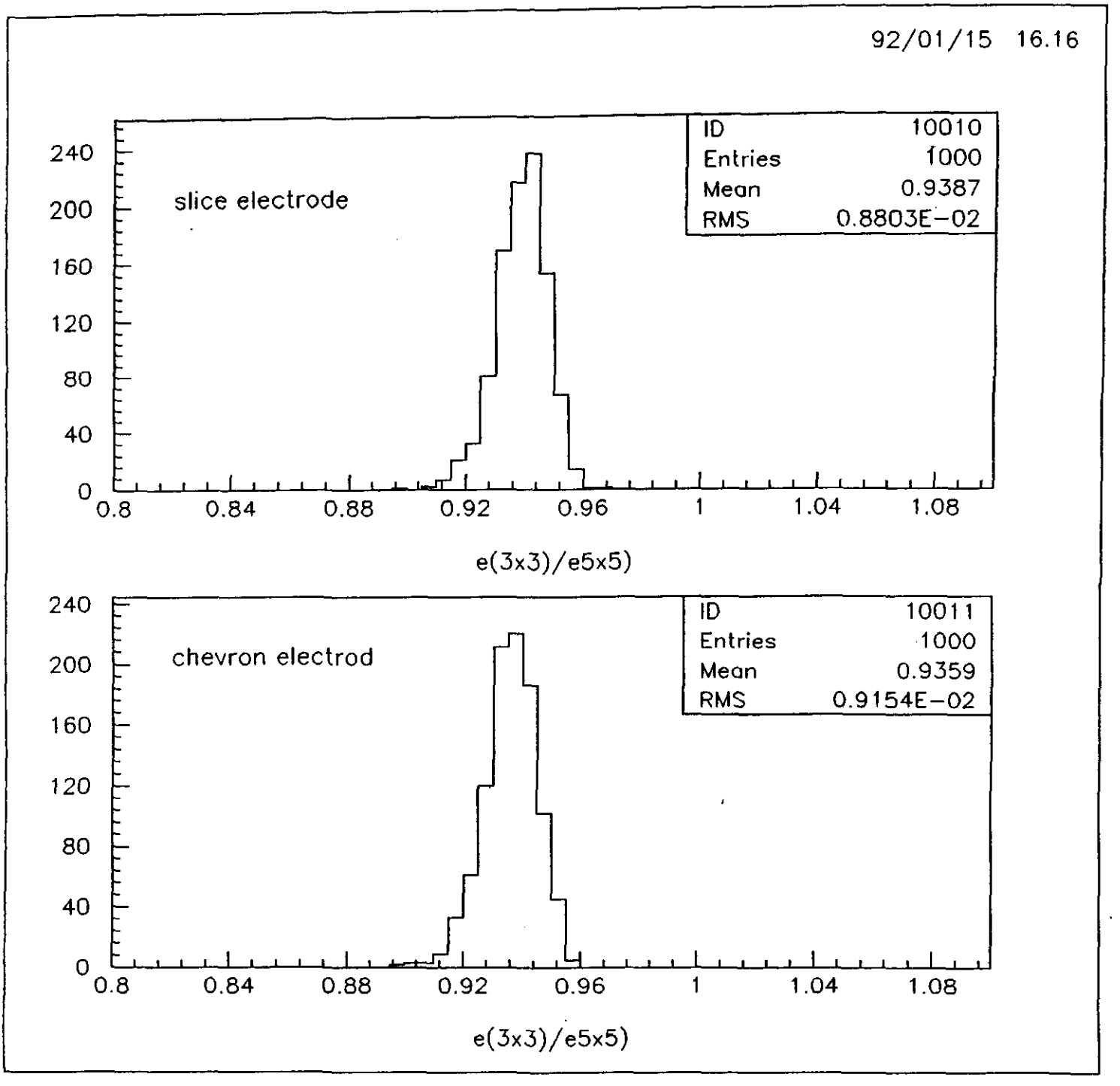
92/01/15 16.16
slice electrode
ID 10010
Entries 1000
Mean 0.9387
RMS 0.8803E-02
240
200
160
120
80
40
0
0.8
0.84
0.88
0.92
0.96
1
1.04
1.08
e(3x3)/e5x5)
chevron electrod
ID 10011
Entries 1000
Mean 0.9359
RMS 0.9154E-02
240
200
160
120
80
40
0
0.8
0.84
0.88
0.92
0.96
1
1.04
1.08
e(3x3)/e5x5)

Figure 10

Figure 11

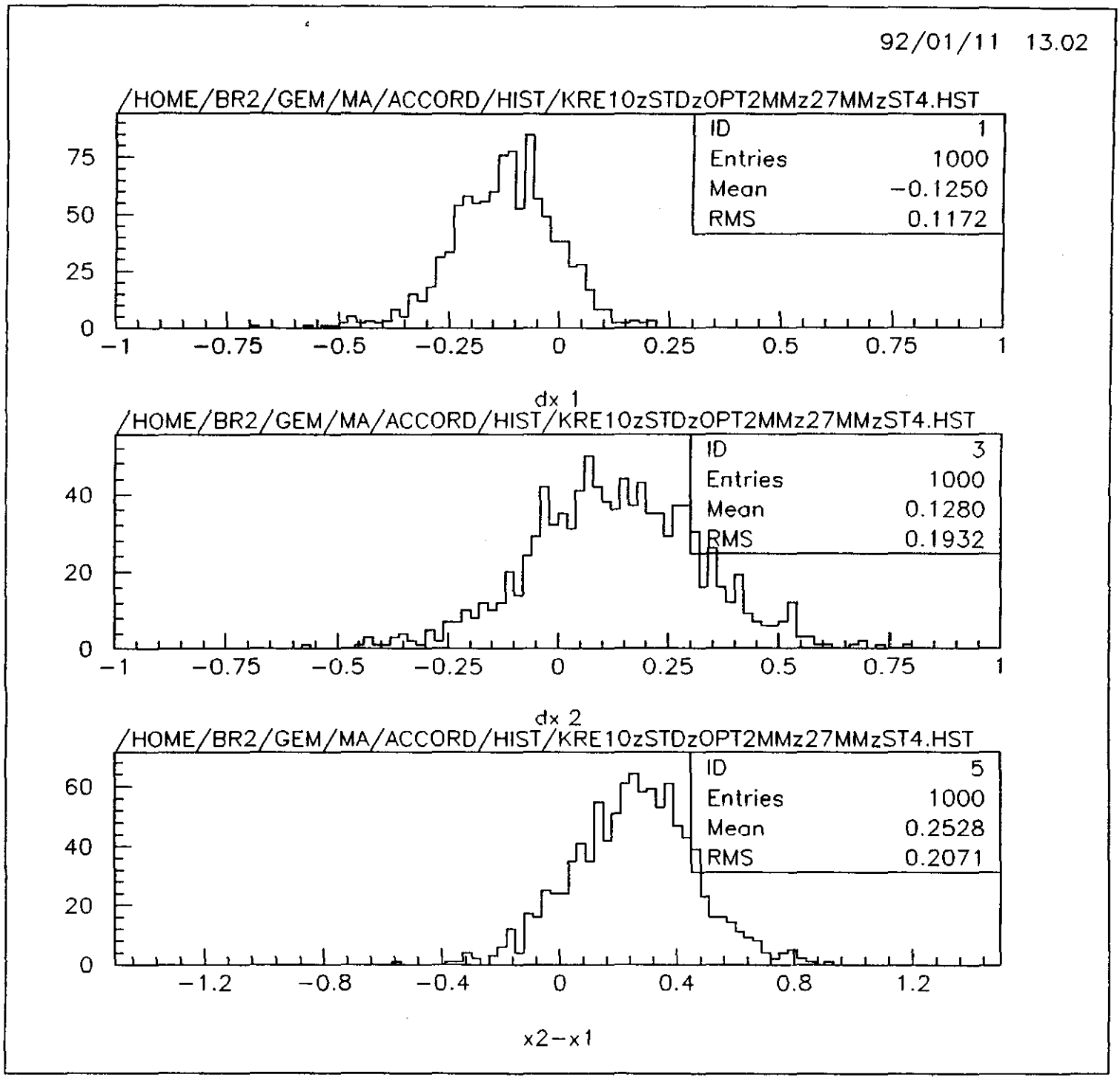
92/01/11 13.02
/HOME/BR2/GEM/MA/ACCORD/HIST/KRE10zSTDzOPT2MMz27MMzST4.HST
ID 1
Entries 1000
Mean −0.1250
RMS 0.1172
dx 1
/HOME/BR2/GEM/MA/ACCORD/HIST/KRE10zSTDzOPT2MMz27MMzST4.HST
ID 3
Entries 1000
Mean 0.1280
RMS 0.1932
dx 2
/HOME/BR2/GEM/MA/ACCORD/HIST/KRE10zSTDzOPT2MMz27MMzST4.HST
ID 5
Entries 1000
Mean 0.2528
RMS 0.2071
x2−x1

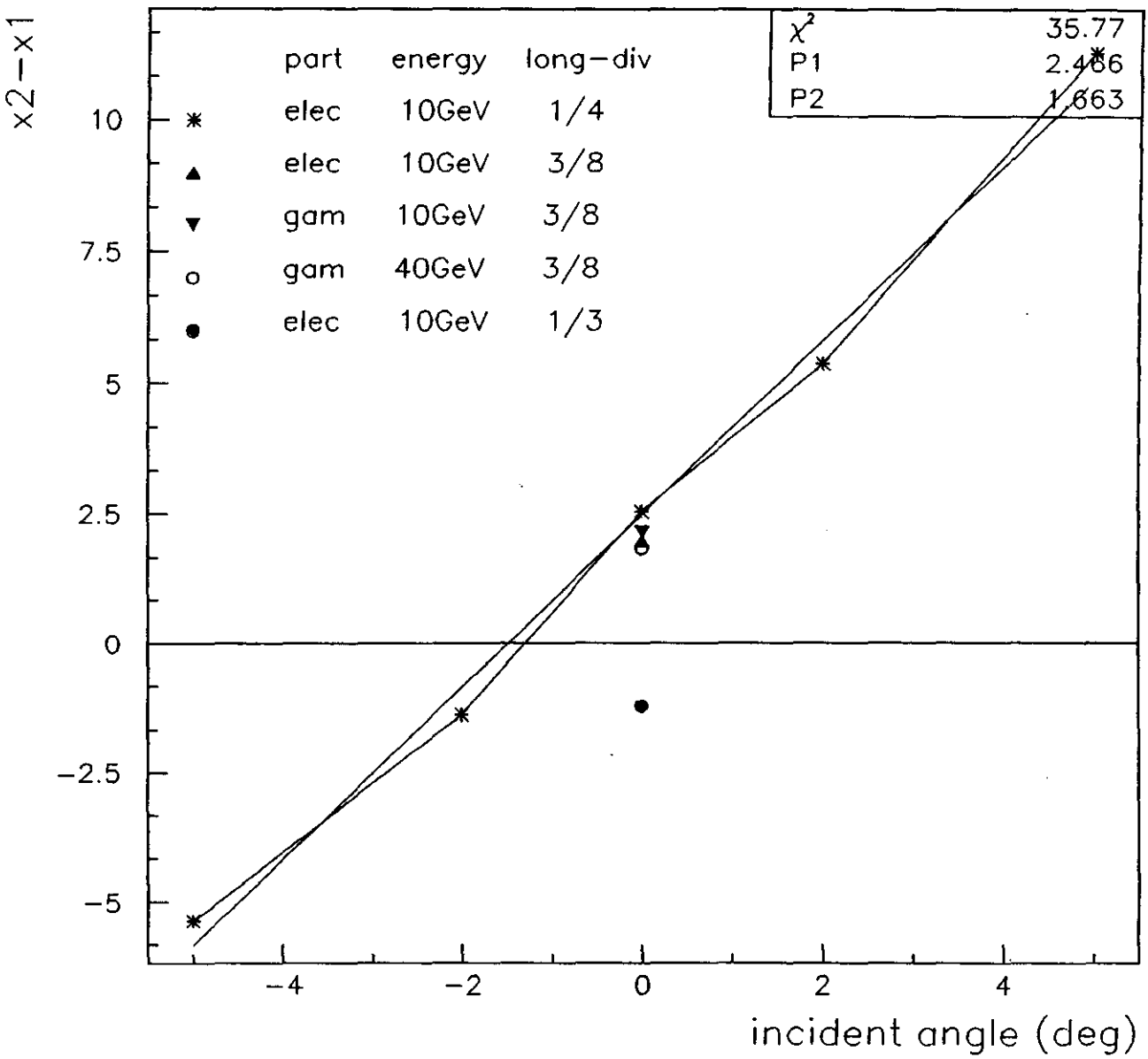
x2−x1
10
7.5
5
2.5
0
−2.5
−5
−4
−2
0
2
4
incident angle (deg)
part energy long−div
elec 10GeV 1/4
elec 10GeV 3/8
gam 10GeV 3/8
gam 40GeV 3/8
elec 10GeV 1/3
χ² 35.77
P1 2.486
P2 1.663

Figure 12

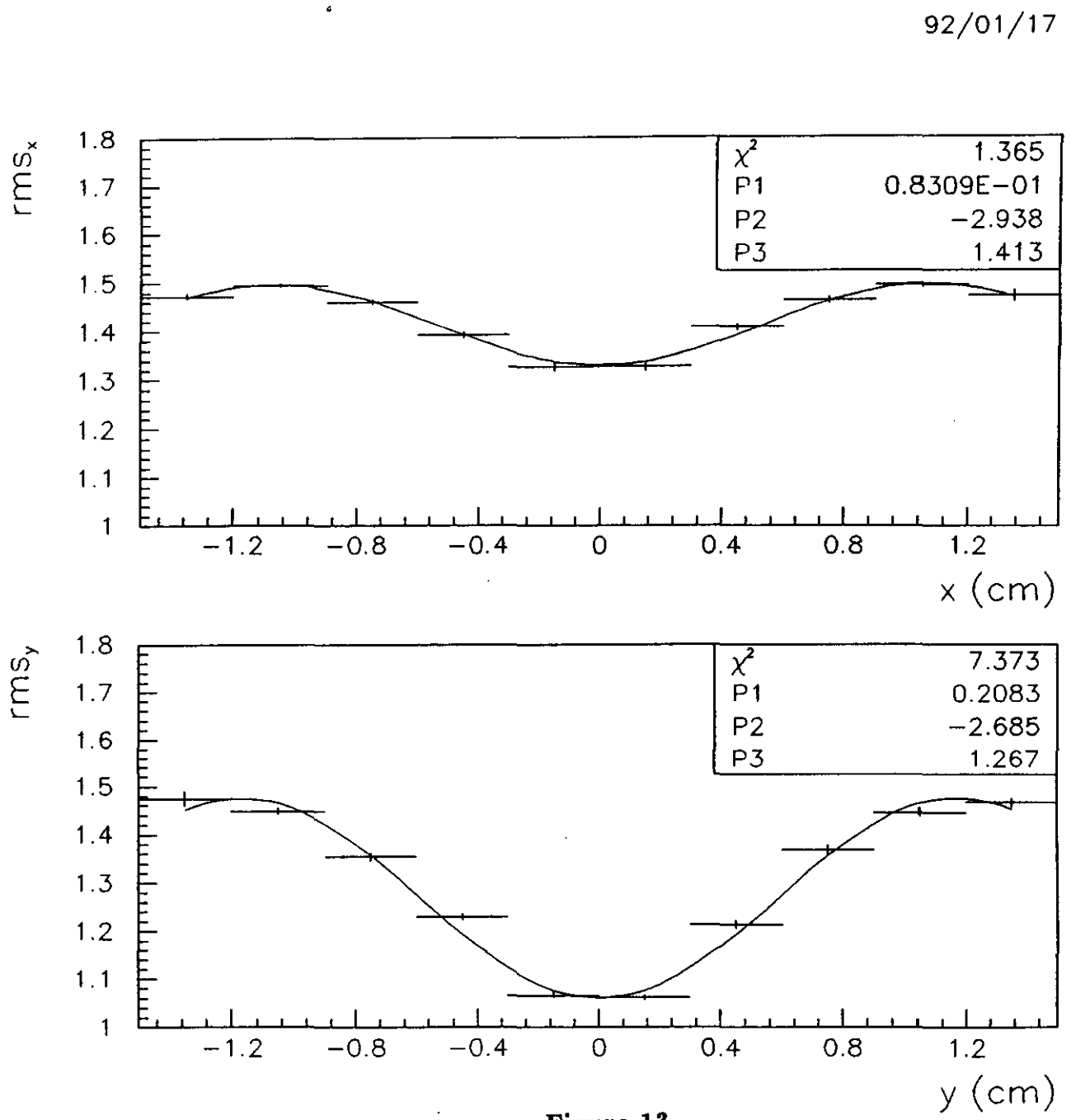
92/01/17 12.33
rms$_x$
1.8
1.7
1.6
1.5
1.4
1.3
1.2
1.1
1
χ^2 1.365
P1 0.8309E−01
P2 −2.938
P3 1.413
−1.2
−0.8
−0.4
0
0.4
0.8
1.2
x (cm)
rms$_y$
1.8
1.7
1.6
1.5
1.4
1.3
1.2
1.1
1
χ^2 7.373
P1 0.2083
P2 −2.685
P3 1.267
−1.2
−0.8
−0.4
0
0.4
0.8
1.2
y (cm)

Figure 13

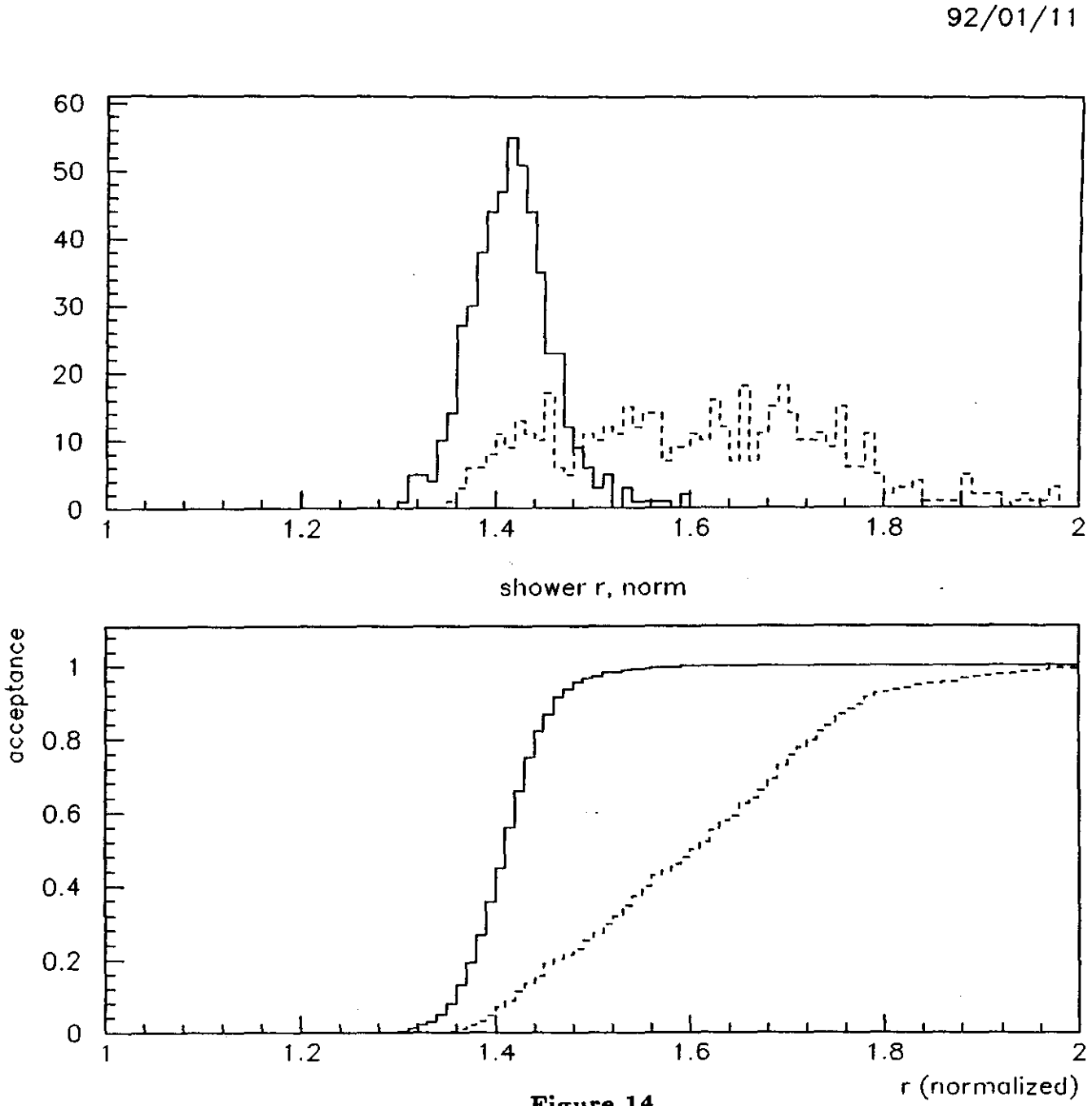
92/01/11 13.41
60
50
40
30
20
10
0
1
1.2
1.4
1.6
1.8
2
shower r, norm
acceptance
1
0.8
0.6
0.4
0.2
0
1
1.2
1.4
1.6
1.8
2
r (normalized)

Figure 14

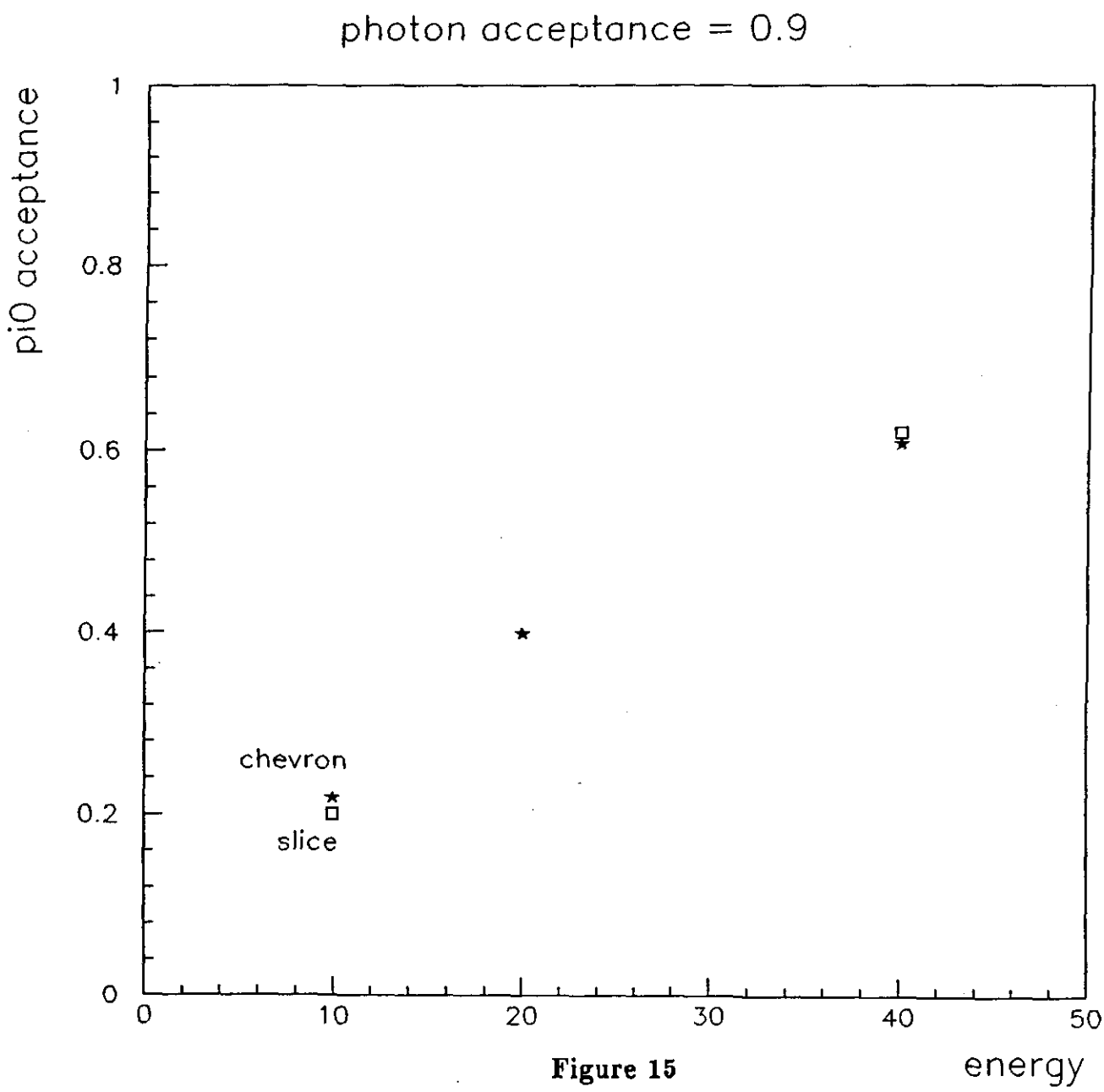
photon acceptance = 0.9
pi0 acceptance
1
0.8
0.6
0.4
0.2
0
0
10
20
30
40
50
energy
chevron
slice

Figure 15

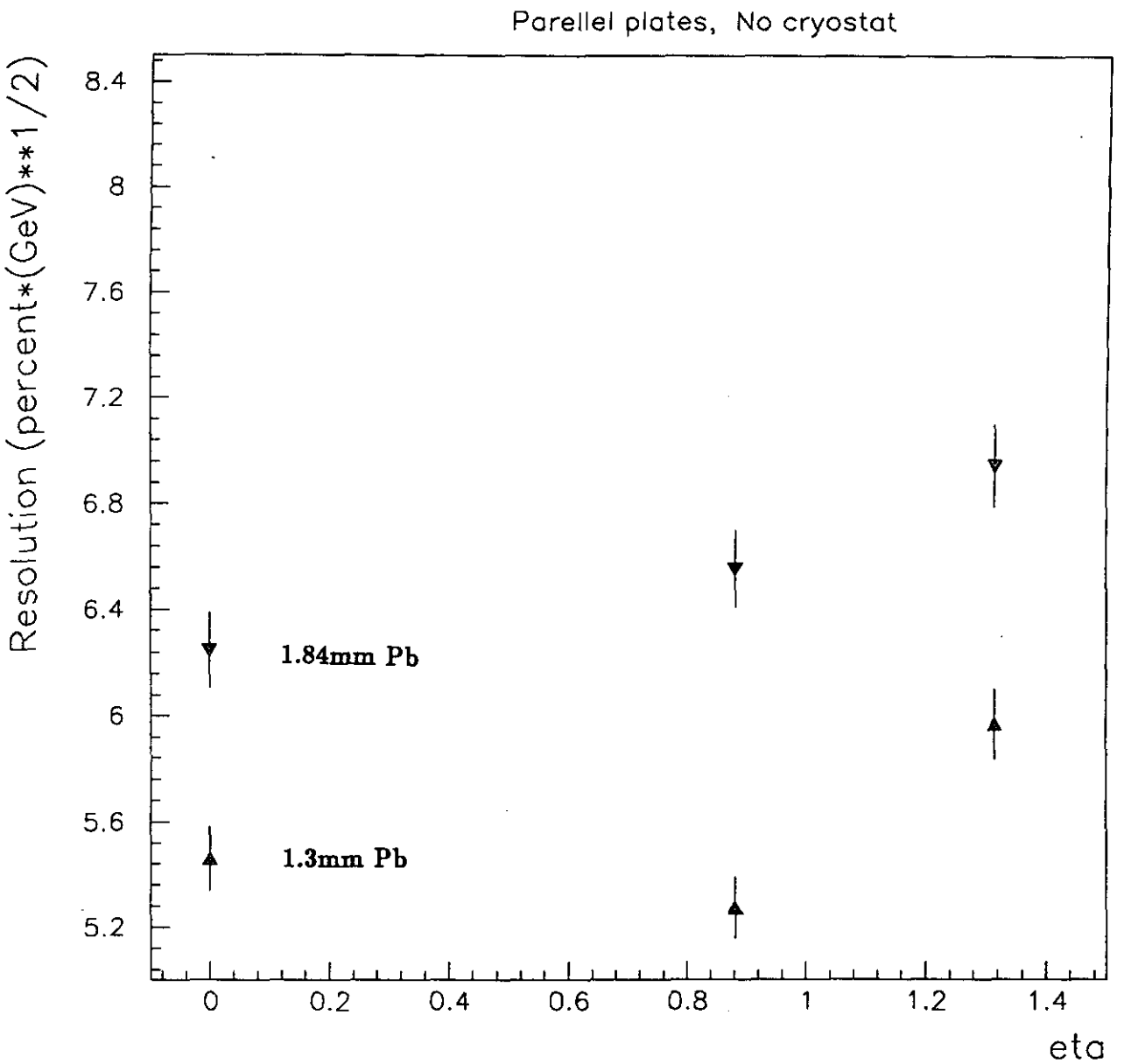
Parellel plates, No cryostat
Resolution (percent*(GeV)**1/2)
8.4
8
7.6
7.2
6.8
6.4
6
5.6
5.2
1.84mm Pb
1.3mm Pb
0
0.2
0.4
0.6
0.8
1
1.2
1.4
eta

Figure 16

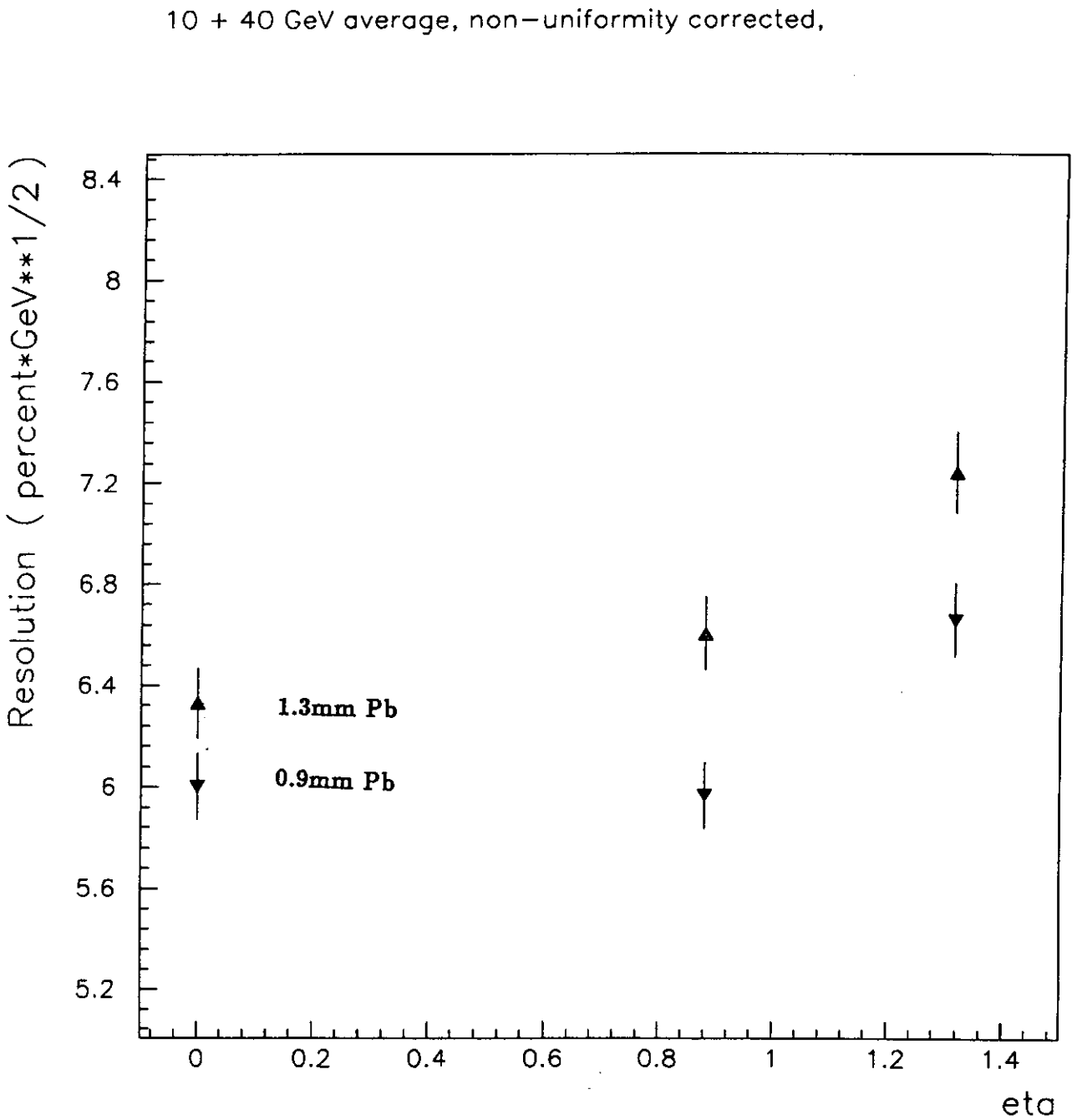
10 + 40 GeV average, non−uniformity corrected,
Resolution (percent*GeV**1/2)
8.4
8
7.6
7.2
6.8
6.4
6
5.6
5.2
1.3mm Pb
0.9mm Pb
0
0.2
0.4
0.6
0.8
1
1.2
1.4
eta

Figure 17

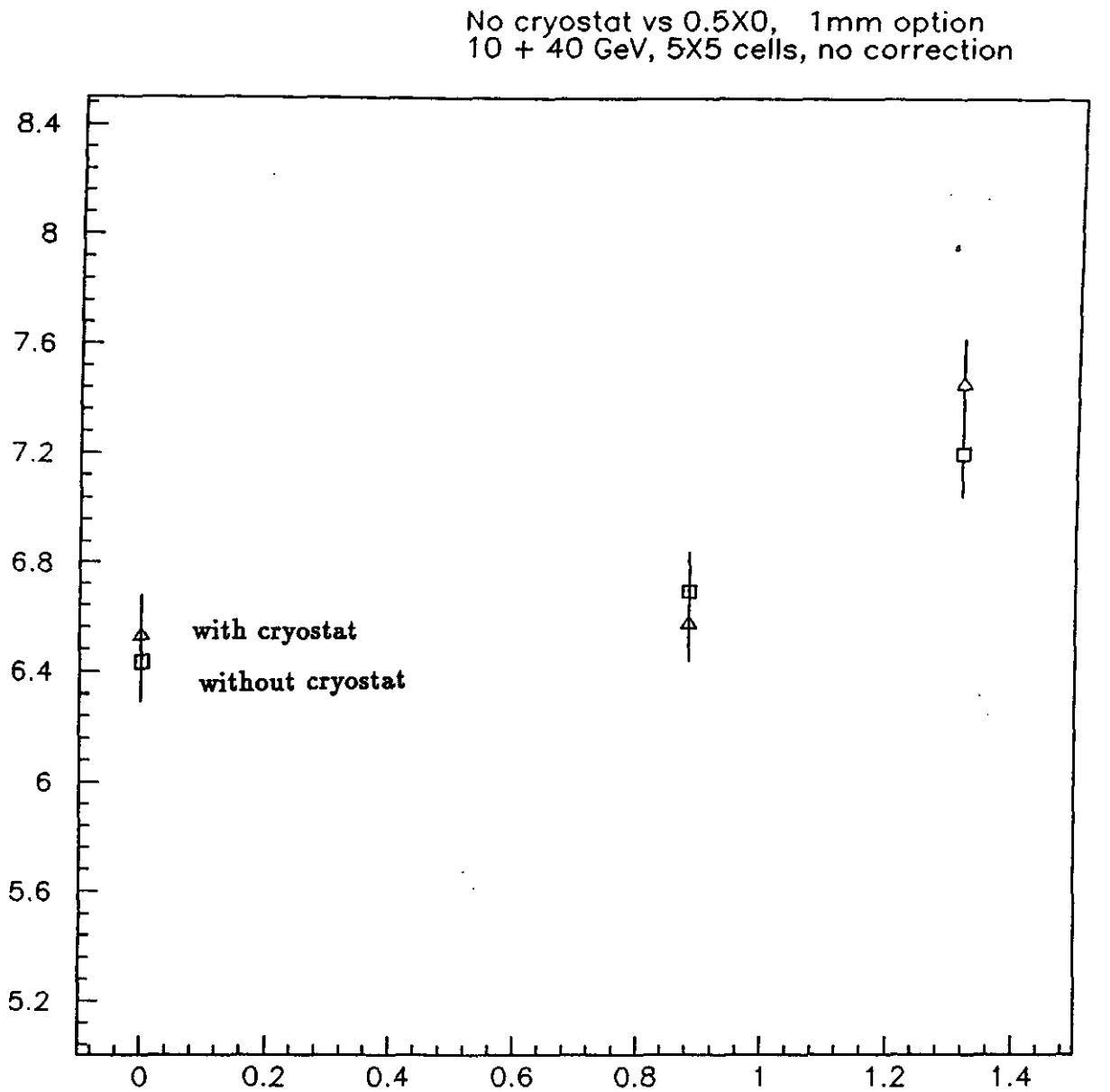
No cryostat vs 0.5X0, 1mm option
10 + 40 GeV, 5X5 cells, no correction
8.4
8
7.6
7.2
6.8
6.4
6
5.6
5.2
0
0.2
0.4
0.6
0.8
1
1.2
1.4
with cryostat
without cryostat

Figure 18

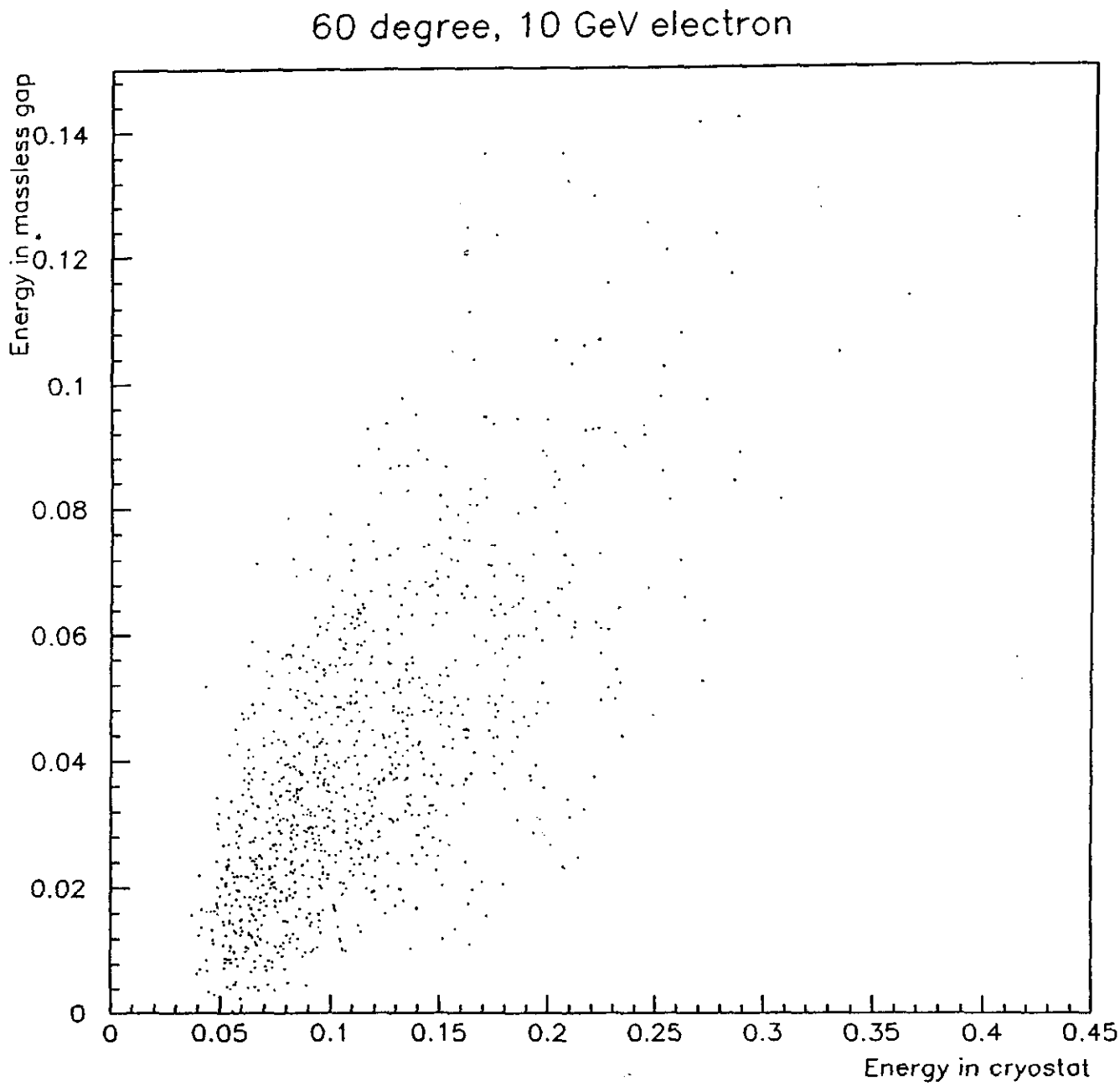
60 degree, 10 GeV electron
Energy in massless gap
0.14
0.12
0.1
0.08
0.06
0.04
0.02
0
0
0.05
0.1
0.15
0.2
0.25
0.3
0.35
0.4
0.45
Energy in cryostat

Figure 19

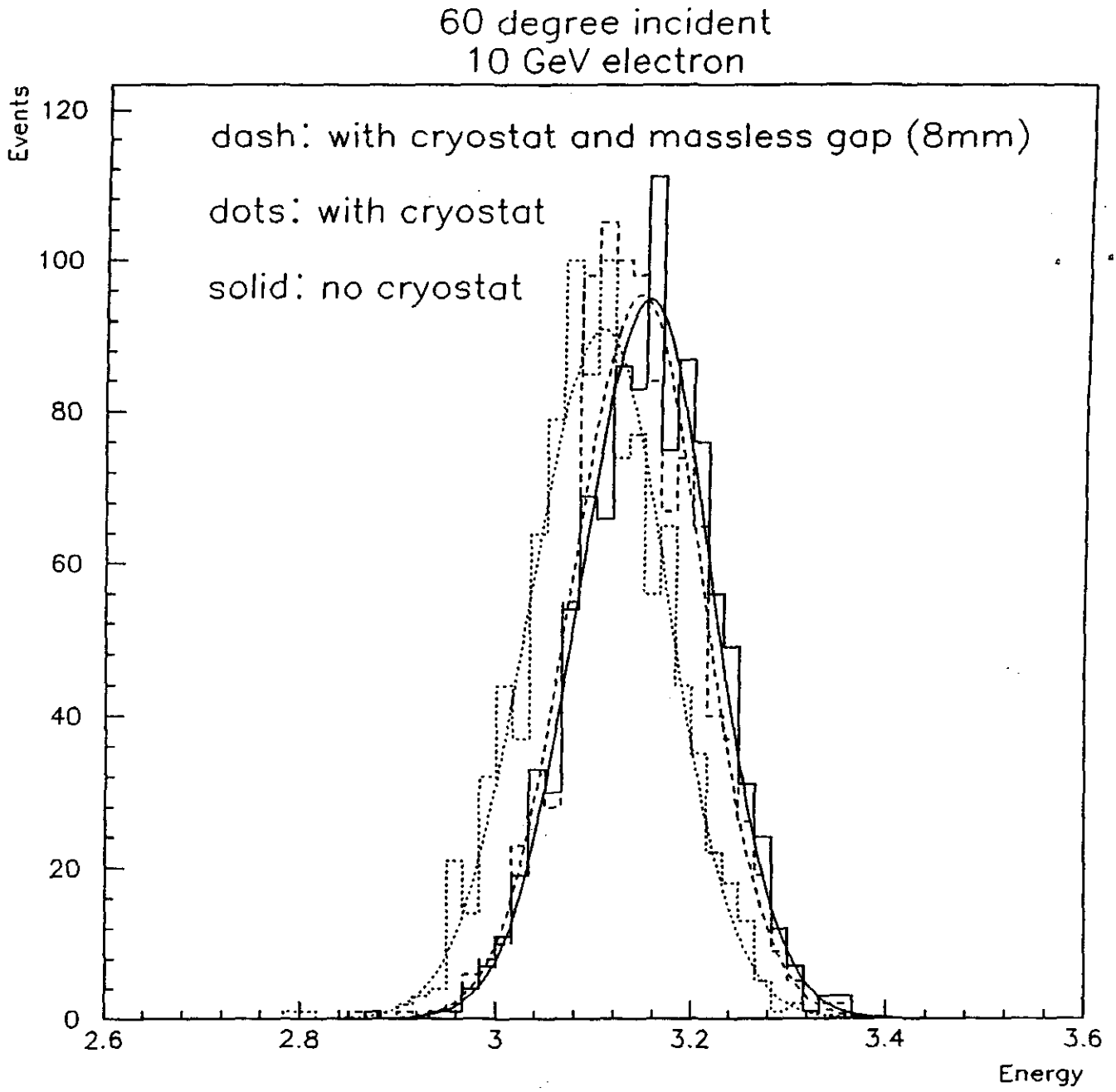
60 degree incident
10 GeV electron
dash: with cryostat and massless gap (8mm)
dots: with cryostat
solid: no cryostat
Events
120
100
80
60
40
20
0
2.6
2.8
3
3.2
3.4
3.6
Energy

Figure 20